九州大学大学院総合理工学府報告
第 37 巻 第 1 号 1-7 頁 平成 27 年 9 月

Engineering Sciences Reports, Kyushu University
Vol. 37, No. 1, pp. 1-7, SEP., 2015

Aerodynamic effect of overhang on a turbulent flow field within a two-dimensional street canyon

Mohd Faizal MOHAMAD[*1,2†], Aya HAGISHIMA[*3], Naoki IKEGAYA[*3], Jun TANIMOTO[*3], and Abd Rahman OMAR[*1]
[†]E-mail of corresponding author: faizal3744@salam.uitm.edu.my

(Received August 25, 2015, accepted August 28, 2015)

This paper reports the results of flow field analysis within and above a two-dimensional street canyon with various overhang lengths using large-eddy simulation (LES). Simulations were conducted for a constant canyon aspect ratio of $W/H = 3$, where W is the street width and H is the building height. Three different overhang lengths were simulated with $P = 0H$, $0.5H$, and $1H$ in order to derive the mean and instantaneous flow characteristics. The results are compared with wind tunnel experiments for validation. The LES results of the mean flow with the $P = 0H$ condition agree fairly well with the wind tunnel data. However, profiles of the standard deviation for the streamwise and vertical velocity components show large discrepancies at all measured locations. In addition, an increase in overhang length on both building façades significantly modifies the in-canyon flow pattern by limiting the penetration of the bulk flow into the canyon layer.

Key words: *Large-eddy simulation (LES), overhang, street canyon, air exchange rate (ACH)*

1. Introduction

The turbulent flow nature of urban street canyons has for decades been a major area of interest within the fields of urban climatology, wind engineering, and building environmental engineering because of its significant effects on the comfort and safety of the urban population relating to urban air quality, thermal comfort, and damage from strong gusts. Although the flow field of a real urban street is highly complicated and varies with urban topography, it has been known that several geometric parameters relating to the building packing density could describe a key feature, namely, the transition of the flow regime. For example, DePaul et al.[1)] revealed that the flow pattern is strongly affected by the aspect ratio W/H (ratio of street width to the building height). Oke[2)] categorized three characteristic flow regimes under different aspect ratios, namely, skimming, wake interference, and isolated roughness flow. Hunter et al.[3)] also investigated the flow structures of uniform building arrays under different conditions of the street aspect ratio, on the basis of a numerical simulation. In addition, Sini et al.[4)] examined the influence of street canyon aspect ratio along with thermal conditions on the in-canyon flow structure and pollutant transport, and revealed that these two factors are strongly related to the number of mean flow vortices, and thus significantly affects the vertical transport process.

In addition to these studies which focused on generic idealized urban geometry, Rafailidis[5)] conducted a wind tunnel experiment on the influence of pitched roofs on the in-canyon flow pattern, which shows that pitched roofs are more effective for enhancing the ventilation within the street canyon compared to wide building spacing.

Meanwhile, in addition to the building packing density and roof shape, various architectural and urban elements with much smaller size compared to buildings have been recognized as secondary urban roughness affecting urban canopy flow. Building overhangs, which we focused on this study, is one of these elements, and commonly seen in tropical climates for protection from direct solar radiation and rain. Foroushani et al.[6)] revealed that an overhang on a building façade

*1 Universiti Teknologi MARA (UiTM)
*2 Department of Energy and Environmental Engineering, Graduate student
*3 Department of Energy and Environmental Engineering

significantly disturbed the flow pattern around the building. Peren et al.[7] investigated ventilation performance in buildings with various configurations of overhang position and inclination angle. Both studies were performed upon an isolated building using Reynolds-averaged Navier Stokes (RANS) simulations. Furthermore, Mohamad et al.[8] conducted a series of RANS simulations of the flow over a two-dimensional (2D) street canyon, and demonstrated that a porch overhanging from a building wall over a 2D street canyon drastically changes the well-known canopy flow regimes such as skimming, wake interference, and isolated flow. These studies on the effect of overhangs on the mean flow field of an urban street canyon suggest that secondary urban roughness can significantly hinder urban ventilation in some cases in spite of its small volume compared to buildings, and raises the necessity for improvement of the transport modelling of the urban canopy layer.

Under these circumstances, the authors of the present study investigated how an overhang affects the characteristics of the turbulent flow within an idealized 2D street canyon in order to deepen the understanding of the relation between the urban ventilation and the urban geometry, on the basis of the computational fluid dynamics (CFD) technique. For reproducing the unsteady flow fluctuation in the canyon, large-eddy simulation (LES) was adopted for the study.

2. Computational settings

2.1 Governing equations

The filtered continuity and Navier–Stokes equations for unsteady incompressible flow are written as

$$\frac{\partial \overline{u_i}}{\partial x_i} = 0 \qquad (1)$$

$$\frac{\partial \overline{u_i}}{\partial t} + \frac{\partial \overline{u_i}\,\overline{u_j}}{\partial x_j} = -\frac{\partial \overline{p}}{\partial x_i} + \nu \frac{\partial^2 \overline{u_i}}{\partial x_j \partial x_j} - \frac{\partial \tau_{ij}}{\partial x_j} \qquad (2)$$

where $\overline{u_i}$ and $\overline{p}$ are filtered velocity and pressure, respectively, and ν is the fluid kinematic viscosity. Here i, j =1, 2 and 3 indicate the streamwise, spanwise, and vertical directions, respectively. τ_{ij} represents the subgrid-scale (SGS) Reynolds stress.

The SGS stress was modelled by the standard Smagorinsky model with Smagorinsky's constant Cs of 0.12. All the simulations were carried out using the open-source CFD code OpenFOAM 2.0.

2.2 Simulation domain

The computational domain adopted in the simulation is shown in Fig. 1. It consists of one idealized 2D street canyon with a building height H of 25 mm, and a street width W of 75 mm, and an aspect ratio W/H of 3 for all three cases. The height of the domain was set to $6H$ as proposed by Franke et al.[9] and Tominaga et al.[10], and the spanwise domain length was kept at $2H$.

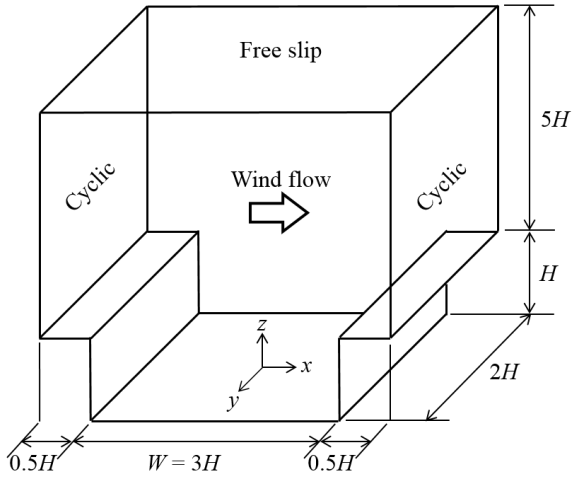

Fig. 1. Schematic of the computational domain adopted in this study.

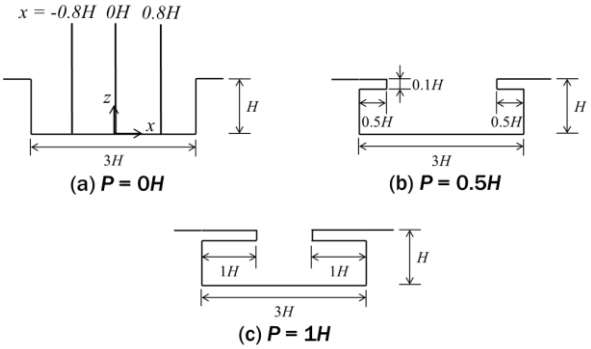

Fig. 2. Configurations of simulated urban street; (a) case: P = 0H, (b) case: P = 0.5H, and (c) case: P = 1H. The three vertical lines included in (a) refer to the positions of vertical profiles shown in Fig. 3.

Figure 2 shows the three calculation cases with different overhang lengths (P= 0H, 0.5H, and 1H). The overhang thickness in each case was set to 0.1H. The domain was discretized

into a uniformly structured mesh with a grid size of $H/16$.

The flow was driven by a pressure gradient, which was aligned in the x direction, so as to maintain the streamwise bulk velocity of 2 m/s. Periodic boundary conditions were employed in the streamwise and spanwise directions to simulate infinitely repeated street canyons at regular intervals. Non-slip boundary conditions were applied on the lower walls and building surfaces, and free slip boundary conditions were imposed on the velocity components at the top boundary, where the velocity normal to the boundary equals zero and the gradient of velocity parallel to wall should be zero.

3. Results and discussion

3.1 Model validation

The vertical profiles of the mean velocities and standard deviations at three different locations ($x = -0.8H$, $0H$, and $0.8H$) for cases with no overhang are shown in Figs. 3 and 4. The data obtained in the wind-tunnel experiment based on the particle image velocimetry (PIV) technique[11] are also included for a comparison. The height and the velocity are normalised by the building height H and reference velocity u_{ref} at a height of $2H$.

The mean velocity profiles derived from the present LES show generally good agreement with the wind tunnel results except for the vertical velocity within the canopy at $x = -0.8H$ and $0.8H$. Considering the relatively small values of the vertical velocity compared to the streamwise component, it is supposed that the discrepancy shown in Figs. 3(d) and 3(f) is acceptable and the current LES properly reproduces the mean flow field within and above the street canyon.

On the other hand, the standard deviations σ_u and σ_w at all the three positions derived from the LES are much smaller than those of the wind tunnel experiment, as seen in Fig. 4. One possible reason for this underestimation of the turbulent intensity in the LES is the small computational domain of the present simulation, which includes only one street canyon. The periodic boundary condition applied on the streamwise boundaries can seemingly reproduce the flow over a horizontally infinite 2D canopy; however, the development of the instantaneous turbulent structure is restricted by the streamwise domain size, as Kanda et al.[12] mentioned. Nevertheless, the shapes of the LES profiles are qualitatively similar to those obtained by the wind tunnel.

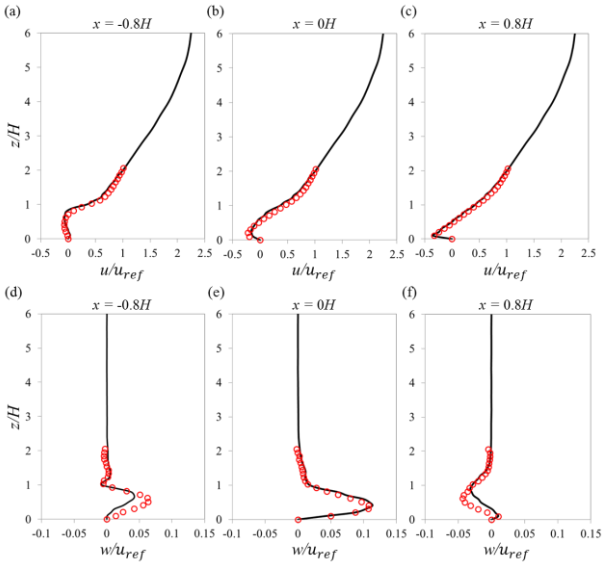

Fig. 3. Vertical distributions of (a)(b)(c) u and (d)(e)(f) w for the case with no overhang. The data of (a) and (d) are at $x = -0.8H$, those of (b) and (e) are $0H$, and (c) and (f) are at $0.8H$ at the lateral centre of the street ($y = 0H$). The solid line refers to the present simulation result, and the open circles refer to the data of the wind tunnel experiment[11]

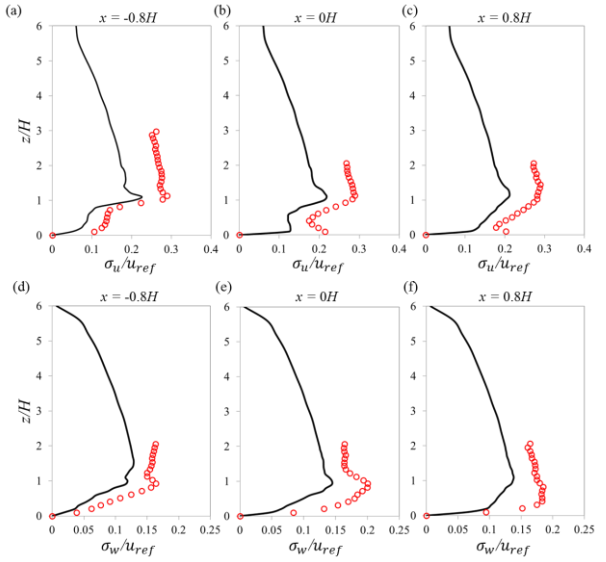

Fig. 4. Vertical distributions of (a)(b)(c) σ_u and (d)(e)(f) σ_w for the case with no overhang. The data of (a) and (d) are at $x = -0.8H$, those of (b) and (e) are $0H$, and (c) and (f) are at $0.8H$ at the lateral centre of the street ($y = 0H$). The solid line refers to the present simulation result, and the open circles refer to the data of the wind tunnel experiment[11]

3.2 Spatially averaged profiles of turbulent statistics

Figure 5 shows the vertical distributions of the spatially averaged mean streamwise velocity, standard deviations of streamwise and vertical velocities, and Reynolds stress.

The streamwise mean velocity for the case with no overhang (Fig. 5(a)) shows negative values at the lower half of the cavity, probably due to the well-known canopy flow regime of wake interference flow. In contrast, the mean velocities for the other two cases with overhang are closer to zero because of the limited area of penetration of the above flow into canyon layer. The velocity gradient immediately above the building height of all the three cases is much larger than that within the canopy layer. It is caused by the strong shear acting on the roof and overhang.

With regard to the standard deviation of streamwise velocity, a peak can be observed at the roof height, and the values decrease as the height increases for all three cases (Fig. 5(b)). Comparing the three cases reveals that the values of σ_u decrease from the case with no overhang to the case with longer overhang, and the peak near the building height becomes steep for the case with longer overhang.

In contrast, the profiles of σ_w show more moderate positive peaks at approximately $1.3H$ compared to the data of σ_u. Similar tendency is shown for σ_w (Fig. 5(c)), where the values decrease with the increase in overhang length.

The profile of the Reynolds stress of the case with no overhang shows a well-known dogleg shape, and a peak appears at the roof height (see Fig. 5(d)). In contrast, the cases with overhang show a strong reduction of the Reynolds stress inside the cavity.

3.3 Time-averaged flow fields

Figure 6 shows the time-averaged velocity structures in the x-z plane at the centre of the lateral position of the domain ($y = 0H$) for all cases. The result of the case with no overhang (Fig. 6(a)) shows a clockwise-rotating primary vortex within the canyon, which is driven by the flow above the building. A secondary anticlockwise-rotating vortex can be also observed at the lower corner of the upstream building. This flow structure can be classified as the wake-interference flow, and is nearly consistent with the results of previous research[2,4].

In contrast, when $P = 0.5H$ (Fig. 6(b)), the cavity is occupied by three vortices. The primary vortex is smaller than that for the case without overhang because it is compressed in the streamwise direction. The secondary vortex developed in front of the upstream building façade extends its size almost twofold in the vertical direction. At the upper corner of the downstream building, a tertiary vortex is observed as the overhang enforces downward flow, resulting in flow separation at the edge of the overhang.

The increase in overhang length further modifies the in-canyon flow pattern as shown in Fig. 6(c). The size of the primary vortex developed at the middle of the canyon is almost the same with the building height in the horizontal and vertical directions. In addition, almost the same size of anticlockwise-rotating vortices exists under both overhangs. The modification of the in-canyon flow pattern by the varied overhang length is consistent with results of Mohamad et al.[8]

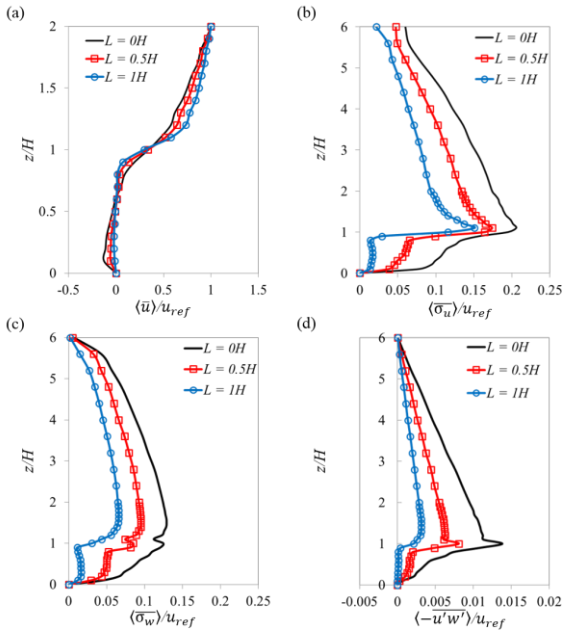

Fig. 5. Vertical distributions of spatially averaged turbulent statistics: (a) streamwise mean velocity, (b) standard deviations of streamwise velocity, (c) standard deviations of vertical velocity, and (d) Reynolds stress for three cases with overhang length P=0H, 0.5H, and 1H.

3.4 Spatial distributions of turbulent statistics

Figure 7 shows the contour maps of the

Reynolds stress in the same x-z plane of Fig. 6. For the case of $P = 0H$ (Fig. 7(a)), a horizontally elongated region with large Reynolds stress is observed at the building height. This feature indicates strong shear between within and above the canyon layer. For $P = 0.5H$ (Fig. 7(b)), the protruding overhangs in both façades restrict the penetration of the upper air into the street canyon, resulting in a smaller region with large Reynolds stress. In the longest overhang case ($P = 1H$) (see Fig. 7(c)), the Reynolds stress of the entire domain is much smaller than the others, and only a weak peak area can be observed at the edge of the downstream overhang. This suggests that the horizontal porches projected out at the upper edge of the building walls work as a part of the secondary earth surface, and make the flow above the building canopy behave like that over a smooth surface where drag force is much smaller than that of ordinary block arrays.

The spatial distributions of the standard deviations σ_u and σ_w for the three cases are shown in Fig. 8. In the case with no overhang, a peak region appears above the street at the building height, similar to the distribution pattern of the Reynolds stress, and this relatively high σ_u area extends downward at the downwind-half portion of the cavity. This is consistent with the vortex generated by the downward flow shown in Fig. 6(a). The wake region near the wall of the upwind building exhibits a small σ_u. In contrast, the data of the case with medium overhang length clearly exhibits the obstruction of the flow penetration into the cavity, and the σ_u values over almost the entire cavity become small. In the case of the longer overhang, the overhang more strongly works to separate the flow within and above the canopy layer. The standard deviation of the vertical velocity σ_w exhibits a similar tendency to the effect of overhang.

Figure 9 shows the distributions of the skewness of streamwise (S_u) and vertical (S_w) velocities. For $P = 0H$ (Fig. 9(a)), S_u is positive in most of the canyon with a peak observed at the lower corner of the upstream building. In contrast, negative S_u is observed in the wake region behind the upstream building. This suggests that the relatively high-speed motion of the vortex penetrates the canyon along with the mean flow pattern at low frequency. The values of S_u and S_w at the building height are in general positive and negative, respectively. This tendency implies that the sweep event with high-speed downward motion is dominant, as shown in past research.

Regarding the data for the case with shorter overhangs, the positive peak of S_u becomes more evident and narrow. It is supposed that the relatively high-speed upper air often penetrates at the building height between the two overhangs, similar to the case with no overhang, but this flow motion toward the cavity is restricted by the overhangs, thus resulting in the narrower regions of both positive S_u and negative S_w.

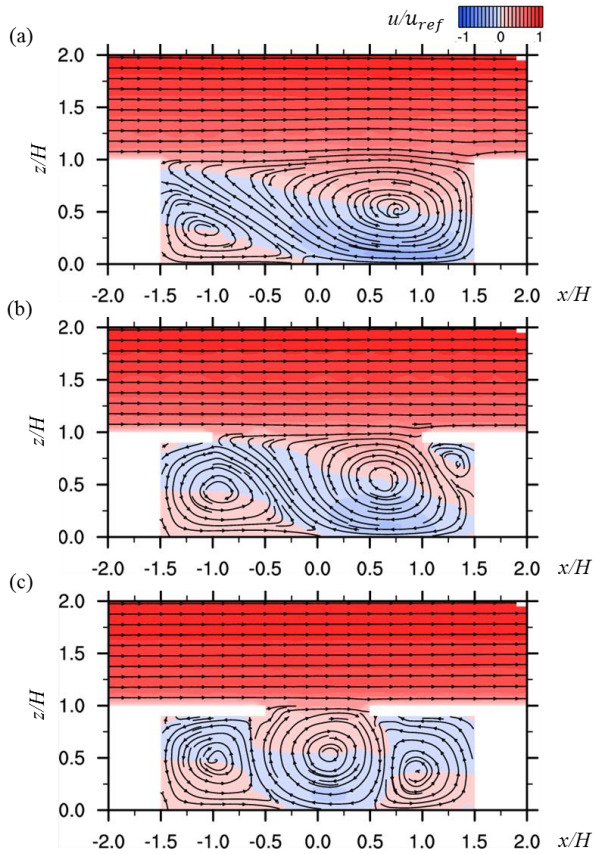

Fig. 6. Normalised velocity contours and streamlines of mean flow in the x-z plane at the middle of the street canyon ($y = 0H$) for (a) $P = 0H$, (b) $P = 0.5H$, and (c) $P = 1H$. The prevailing wind is to the right.

The distributions of skewness for the case of $P = 1H$ are much more complex compared to the aforementioned two cases; thus, it is difficult to simply describe the features. However, the regions of positive S_u and negative S_w elongating from between the gap of overhangs obliquely downward can still be observed. They imply the sweep motion dominates the ventilation of the cavity beneath the overhangs.

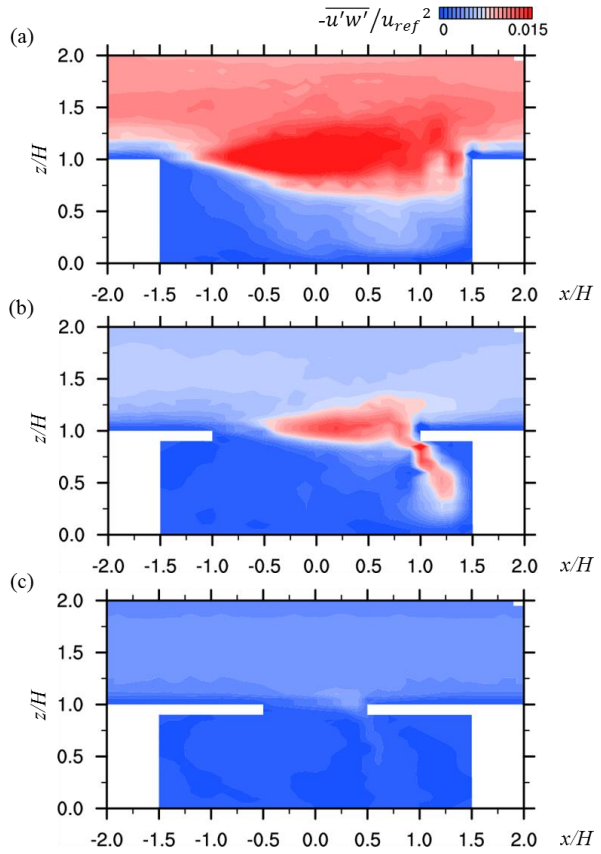

Fig.7. Normalised Reynolds stress in the x-z plane at the middle of the street canyon ($y = 0H$) for (a) $P = 0H$, (b) $P = 0.5H$, and (c) $P = 1H$. The prevailing wind is to the right.

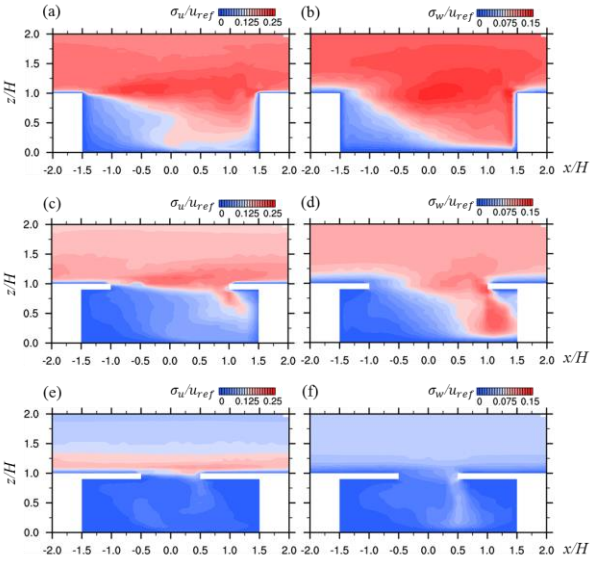

Fig. 8. Contour of normalised standard deviation of streamwise and vertical velocity in the x-z plane through the middle of the street canyon ($y = 0H$) for (a)(b) $P = 0H$, (c)(d) $P = 0.5H$, and (e)(f) $P = 1H$. The prevailing wind is to the right.

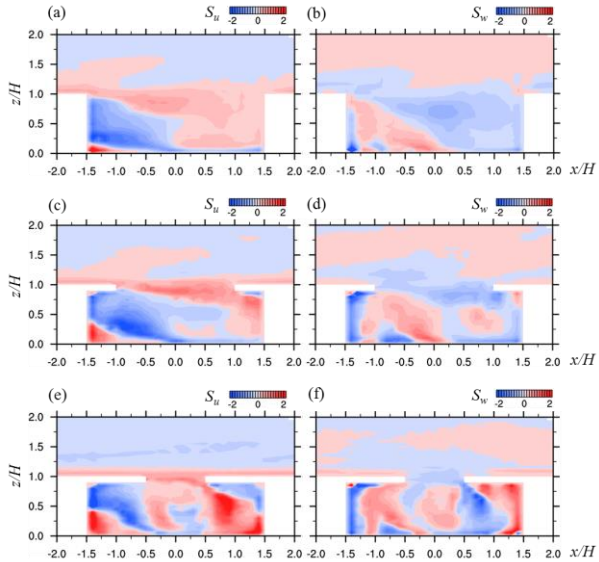

Fig. 9. Contour of spatial distribution of skewness for streamwise and vertical velocity components in the vertical x-z plane through the middle of the street canyon ($y = 0H$) for (a)(b) $P = 0H$, (c)(d) $P = 0.5H$, and (e)(f) $P = 1H$. The prevailing wind is to the right.

4. Conclusion

The LESs of the flow over the 2D street canyon with an aspect ratio of 3 were conducted to investigate the effect of overhang on the turbulent flow field.

The calculation results of the mean flow structure for the case with no overhang indicate that the well-known wake interference flow regime consists of two co-rotating vortices. In contrast, the mean flow for the two cases with overhangs exhibit a remarkable modification of the flow regime with an increased number vortices and an alteration of the vortex size, because protruding overhangs on the building façades restrict the penetration of the upper air into the canyon layer, resulting in a strong reduction of the velocity within the canopy.

It is shown that the Reynolds stress within and near the canopy layer is strongly reduced by the overhangs. In other words, overhangs extended from a building roof act as a projected secondary street surface, which makes the flow above the building behave like that over a smooth wall with small surface drag.

Acknowledgments

This work was supported by JSPS KAKENHI Grant No. 25289196.

References

1) DePaul, F. T., Sheih, C. M. Measurements of wind velocities in a street canyon. Atmos. Environ., 20, 455 (1986).
2) Oke, T. R. Street design and urban canopy layer. Energy Build., 11, 103 (1988).
3) Hunter, L. J., Watson, I. D., Johnson, G. T. Modelling air flow regimes in urban canyons. Energy Build., 15, 315 (1990).
4) Sini, J. F., Anquetin, S., Mestayer, P. G. Pollutant dispersion and thermal effects in urban street canyons. Atmos. Environ., 30, 2659 (1995).
5) Rafailidis, S. Influence of building areal density and roof shape on the wind characteristics above a town. Boundary-Layer Meteorol., 85, 255 (1997).
6) Foroushani, M. S. S., Naylor, D. H. Ge. Effects of roof overhangs on wind-driven rain wetting of a low-rise cubic building: A numerical study. J. Wind Eng. Ind. Aerodyn., 125, 38 (2014).
7) Peren, J. I., van Hooff, T., Leite, B. C. C., Blocken, B. Impact of eaves on cross ventilation of a generic isolated leeward sawtooth roof building: Windward eaves, leeward eaves and eaves inclination. Build. Environ., 92, 578 (2015).
8) Mohamad, M. F., Hagishima, A., Tanimot, J., Ikegaya, N., Omar, A. R. On the effect of various design factors on wind-induced natural ventilation of residential buildings in Malaysia. The 2nd Asia Confer. of Inter. Build. Performance Simulation Assoc. (2014).
9) Franke, J., Hellsten, A., Schlunzen, H., Carissimo, B. editors. Best practice guideline for the CFD simulation of flows in the urban environment. COST Office Brussels (2007).
10) Tominaga, Y., Mochida, A., Yoshie, R., Kataoka, H., Nozu, T., Yoshikawa, M., et al. AIJ guidelines for practical applications of CFD to pedestrian wind environment around buildings. J. Wind. Eng. Ind. Aerodyn., 96, 1749 (2008).
11) Sato, T., Hagishima, A., Ikegaya, N., Tanimot, J. Wind tunnel experiment on turbulent flow field around 2D street canyon with eaves. 9th Inter. Confer. on Urban Climate (2015).
12) Kanda, M., Morikawa, R., Kasamatsu, F. Large-eddy simulation of turbulent organized structures within and above explicitly resolved cube arrays. Boundary-Layer Meteorol., 112, 343 (2004).